AMERICAN SOCIETY FOR MICROBIOLOGY | Journal of Virology

Identification of a Novel Viral Protein Expressed from the PB2 Segment of Influenza A Virus

Seiya Yamayoshi,[a] Mariko Watanabe,[a] Hideo Goto,[a] Yoshihiro Kawaoka[a,b,c,d]

Division of Virology, Department of Microbiology and Immunology, Institute of Medical Science, University of Tokyo, Tokyo, Japan[a]; Department of Pathobiological Sciences, School of Veterinary Medicine, University of Wisconsin–Madison, Madison, Wisconsin, USA[b]; Department of Special Pathogens, International Research Center for Infectious Diseases, Institute of Medical Science, University of Tokyo, Tokyo, Japan[c]; ERATO Infection-Induced Host Responses Project, Japan Science and Technology Agency, Saitama, Japan[d]

ABSTRACT

Over the past 2 decades, several novel influenza virus proteins have been identified that modulate viral infections *in vitro* and/or *in vivo*. The PB2 segment, which is one of the longest influenza A virus segments, is known to encode only one viral protein, PB2. In the present study, we used reverse transcription-PCR (RT-PCR) targeting viral mRNAs transcribed from the PB2 segment to look for novel viral proteins encoded by spliced mRNAs. We identified a new viral protein, PB2-S1, encoded by a novel spliced mRNA in which the region corresponding to nucleotides 1513 to 1894 of the PB2 mRNA is deleted. PB2-S1 was detected in virus-infected cells and in cells transfected with a protein expression plasmid encoding PB2. PB2-S1 localized to mitochondria, inhibited the RIG-I-dependent interferon signaling pathway, and interfered with viral polymerase activity (dependent on its PB1-binding capability). The nucleotide sequences around the splicing donor and acceptor sites for PB2-S1 were highly conserved among pre-2009 human H1N1 viruses but not among human H1N1pdm and H3N2 viruses. PB2-S1-deficient viruses, however, showed growth kinetics in MDCK cells and virulence in mice similar to those of wild-type virus. The biological significance of PB2-S1 to the replication and pathogenicity of seasonal H1N1 influenza A viruses warrants further investigation.

IMPORTANCE

Transcriptome analysis of cells infected with influenza A virus has improved our understanding of the host response to viral infection, because such analysis yields considerable information about both *in vitro* and *in vivo* viral infections. However, little attention has been paid to transcriptomes derived from the viral genome. Here we focused on the splicing of mRNA expressed from the PB2 segment and identified a spliced viral mRNA encoding a novel viral protein. This result suggests that other, as yet unidentified viral proteins encoded by spliced mRNAs could be expressed in virus-infected cells. A viral transcriptome including the viral spliceosome should be evaluated to gain new insights into influenza virus infection.

Influenza A virus has 8 segmented, negative-sense viral RNAs (vRNAs) as its genome (1). In 1977 and 1978, it was reported that each vRNA encodes a major viral protein; these major proteins are PB2, PB1, PA, HA, NP, NA, M1, and NS1 (2–4). Subsequently, M2 and NEP (NS2) were shown to be encoded by spliced mRNAs that are expressed from the M and NS segments, respectively (5–14). Moreover, several other novel viral proteins have been shown to be expressed by splicing, alternative initiation, or ribosomal frameshifts. For example, M42 and NS3 are translated from spliced mRNAs transcribed from the M and NS segments, respectively (15, 16). M42 functions in place of M2 as a proton channel (15), and NS3 is associated with the adaptation of avian influenza A virus to new mammalian hosts (16). Approximately 30 of >18,000 isolates likely express M42 and NS3, based on nucleotide sequence analyses (15, 16). PB1-F2, PB1-N40, PA-N155, and PA-N182 are expressed from alternative translation initiation sites in the PB1 and PA segments (17–21). Although the functions of PB1-N40, PA-N155, and PA-N182 remain unclear, PB1-F2 is associated with pathogenicity, inducing apoptosis and a reduction in the mitochondrial inner membrane potential (17, 22). Reduction of the mitochondrial potential inhibits RIG-I-dependent interferon (IFN) signaling and NOD-like receptor family pyrin domain-containing 3 (NLRP3)-mediated inflammasome formation (23, 24). PA-X, which comprises an N-terminal PA domain (191 amino acids [aa]) and a C-terminal PA-X-specific domain (61 aa), is expressed as a result of a ribosomal frameshift (25). PA-X modulates host immune responses via its shutoff activity (25). Although several novel viral proteins have thus been revealed, other, as yet unidentified viral accessory proteins may also be present in virus-infected cells.

Splicing is regulated primarily by the nucleotide sequence, namely, the splice donor (SD) and splice acceptor (SA) sites (26). Accordingly, all immature mRNAs always have the potential to be edited by splicing. Yet only the M and NS segments are known to encode viral proteins in spliced mRNAs (27). In the present study, we focused on the PB2 segment, which is one of the longest segments of influenza A virus, to explore whether a novel spliced mRNA from the PB2 segment encodes a novel viral protein. We identified a novel viral protein expressed from the PB2 segment and characterized it. We also

Received 26 August 2015 **Accepted** 13 October 2015

Accepted manuscript posted online 21 October 2015

Citation Yamayoshi S, Watanabe M, Goto H, Kawaoka Y. 2016. Identification of a novel viral protein expressed from the PB2 segment of influenza A virus. J Virol 90:444–456. doi:10.1128/JVI.02175-15.

Editor: T. S. Dermody

Address correspondence to Seiya Yamayoshi, yamayo@ims.u-tokyo.ac.jp, or Yoshihiro Kawaoka, kawaokay@svm.vetmed.wisc.edu.

S.Y. and M.W. contributed equally to this article.

evaluated the importance of this novel viral protein for virus replication *in vitro* and pathogenicity in mice.

MATERIALS AND METHODS

Cells. Madin-Darby canine kidney (MDCK) cells were maintained in Eagle's minimal essential medium (MEM) containing 5% newborn calf serum (NCS). Human embryonic kidney 293T and 293 cells, human alveolar adenocarcinoma epithelial A549 cells, mouse L929 cells, and avian DF-1 cells were maintained in Dulbecco's modified Eagle's medium (DMEM) containing 10% fetal calf serum (FCS). MDCK, 293T, 293, A549, L929, and DF-1 cells were incubated at 37°C under 5% CO_2.

Virus preparation by using reverse genetics. Plasmid-based reverse genetics for virus generation was performed as previously described (28, 29). Influenza A/WSN/33 (H1N1; referred to as WSN) virus and its mutant viruses were propagated and titrated in MDCK cells. All viruses were sequenced to confirm the absence of unwanted mutations. A/Puerto Rico/8/34 (H1N1; PR8), A/Kawasaki/173/2001 (H1N1; K173), A/Gunma/07G006/2008 (H1N1; Gunma), A/Osaka/164/2009 (H1N1pdm; Osaka), A/Yokohama/UT-K2A/2011 (H1N1pdm; K2A), A/Aichi/2/68 (H3N2; Aichi), A/Yokohama/UT-K4A/2011 (H3N2; K4A), A/duck/Wisconsin/8/74 (H3N2; WI), and A/duck/Mongolia/301/2001 (H3N2; Mon) were propagated and titrated in MDCK cells.

Construction of plasmids. pCA-PB2, pCA-PB1, pCA-PA, pCA-NP, pCA-NS1, pCA-PB2-FLAG, pCA-PB1-FLAG, pCA-PA-FLAG, and pCA-NP-FLAG were reported previously (28, 29). pPolI-PB2 D(CT), pPolI-PB2 Dsm, pPolI-PB2 A(TC), pPolI-PB2 Asm, pPolI-PB2 DAsm, and pPolI-PB2-S1 were generated by primer-based site-directed mutagenesis based on pPolI-PB2 (28). The open reading frames (ORFs) of these PB2 mutants were subcloned into pCAGGS/MCS for protein expression. pCA-PB2-S1 was generated by using a PCR-based standard technique based on pPolI-PB2. A C-terminal FLAG tag was inserted into pCA-PB2-S1 in frame, resulting in the pCA-PB2-S1-FLAG construct. Mutations or deletions in the PB2-S1 gene were generated by using a PCR-based standard technique. The resulting constructs were named pCA-PB2-S1 L7D, pCA-PB2-S1 Δ1-12, pCA-PB2-S1 Δ1-27, pCA-PB2-S1 L7L10A, and pCA-PB2-S1 N9D.

Viral RNAs were extracted from PR8, K173, Gunma, Osaka, K2A, Aichi, and K4A viruses propagated in MDCK cells by using Isogen-LS (Nippon Gene). cDNAs, obtained by use of a standard reverse transcription-PCR (RT-PCR) technique, were cloned into pCAGGS with an N-terminal FLAG tag. Mutations in the PB2 gene from K173 (K173 DAsm) were generated by using a PCR-based standard technique. The cDNA for RIG-IN, which contains the N-terminal 229 aa of human RIG-I, was isolated by using a standard RT-PCR technique and inserted into pCAGGS with an N-terminal Myc tag, resulting in the pCA-N-Myc-RIG-IN construct. All constructs were sequenced to confirm the absence of unwanted mutations. Primer sequences are available upon request.

Virus inoculation into cultured cells. MDCK, A549, 293, L929, and DF-1 cells were infected with the indicated viruses at a multiplicity of infection (MOI) of 0.001 (for growth kinetics), 0.1 (for immune staining), or 5 to 10 (for other experiments). After incubation at 37°C for 1 h, the viral inoculum was replaced with MEM containing 0.3% bovine serum albumin and tosylsulfonyl phenylalanyl chloromethyl ketone (TPCK)-treated trypsin (1 μg/ml), followed by a further incubation for the indicated times at 37°C.

Transfection. 293 and 293T cells were transfected with the indicated plasmids by use of Trans-IT 293 (TaKaRa Bio) according to the manufacturer's protocol. At 24 h posttransfection, the following experiments were performed.

RT-PCR. Total RNA was extracted from virus-infected or plasmid-transfected MDCK or 293 cells by use of an RNeasy Plus minikit (Qiagen) or Isogen (Nippon Gene). Total RNA extracted from the plasmid-transfected cells was treated with DNase I (Qiagen). Total RNA was then reverse transcribed with an oligo(dT) primer and SuperScript III reverse transcriptase (Life Technologies). To look for a novel spliced mRNA, PCR was performed with 8 different forward primers, i.e., 28F (ATGGAAAG AATAAAAGAACTAAG), 200F (CAGCAGACAAGAGGATAACG), 400F (TTAAAACATGGAACCTTTGG), 600F (AGAACTCCAGGGTTGCAA AATTTC), 800F (GCTTAATTATTGCTGCTAGAAAC), 1000F (TTTGG TGGATTCACATTTAAG), 1200F (ACAGTCGATTGCCGAAGCAATA ATTG), and 1400F (TGGGAATGATCGGGATATTG), and the reverse primer 2307R (CTAATTGATGGCCATCCGAATTCTTTTG), using GoTaq Green master mix (Promega) as follows. After 3 min of denaturation at 98°C, samples were subjected to 40 cycles of amplification, consisting of 30 s at 98°C, 30 s at 50°C, and 90 s at 72°C, with a final additional extension step at 72°C for 5 min. To detect the PB2 mRNA2 in cells infected with 8 human and 2 avian isolates, PCR was performed with the forward primer uniPB2-1388F (ATCGACAATGTGATGGGAATGAT) and the reverse primer 2307R by using GoTaq Green master mix as follows: after 5 min of denaturation at 95°C, samples were subjected to 35 cycles of amplification, consisting of 30 s at 95°C, 30 s at 55°C, and 45 s at 72°C, with a final additional extension step at 72°C for 5 min. For the specific detection of PB2 mRNA1, PB2 mRNA2, and glyceraldehyde-3-phosphate dehydrogenase (GAPDH) mRNA, PCR was performed by using GoTaq Green master mix. To detect PB2 mRNA1, PCR was performed with primers uniPB2-1148F (TCAGAAAAGCAACCAGGAGA TTG) and uniPB2-1619R (GAGTAAGTTATTGTCAGTTTCTC) under the following conditions: 95°C for 5 min; 25 (to confirm specificity), 20 (for virus infection), or 18 (for plasmid transfection) cycles of 95°C for 30 s, 59°C for 30 s, and 72°C for 45 s; and 72°C for 5 min. To detect PB2 mRNA2, PCR was performed with primers uniPB2-1148F and PB2-junctionR (TTTGCTTTGGTGGAGCGGCAC) under the following conditions: 95°C for 5 min; 35 (to confirm specificity), 30 (for virus infection), or 23 (for plasmid transfection) cycles of 95°C for 30 s, 65°C for 30 s, and 72°C for 45 s; and 72°C for 5 min. To detect GAPDH mRNA, PCR was performed with primers human GAPDH-F (TGAAGGTCGGAGTCAAC GGATTTGGT) and human GAPDH-R (CATGTGGGCCATGAGGTCC ACCAC) under the following conditions: 95°C for 5 min; 20 (for virus infection) or 15 (for plasmid transfection) cycles of 95°C for 30 s, 60°C for 30 s, and 72°C for 45 s; and 72°C for 5 min. PCR products were separated in 0.6% to 1% agarose gels and imaged by using Printgraph (Atto) or a Gel Doc EZ system (Bio-Rad). In some cases, the nucleotide sequence of a PCR product was determined by using a model 3130xl genetic analyzer (Life Technologies) and a BigDye Terminator v3.1 cycle sequencing kit (Life Technologies). The plasmids pPolI-PB2 and pPolI-PB2-S1 (10^2 to 10^9 copies/reaction mix) served as controls.

Western blotting. Total cell lysates prepared from plasmid-transfected 293 cells or virus-infected MDCK, A549, 293, L929, or DF-1 cells were loaded onto Any kD Mini-Protean TGX precast gels (Bio-Rad). Separated proteins were transferred to Immobilon-P membranes (Millipore) and probed with two mouse monoclonal antibodies against PB2 (clones 21/3 and 18/1) (30), an anti-PB2-S1 antibody (IBL) which recognizes a WSN PB2-S1-derived peptide (PLHQSKVERSSPH), a rabbit anti-FLAG antibody (Sigma), and the mouse monoclonal anti-ACTB antibody clone AC-74 (Sigma).

***In silico* sequence analysis.** The splicing site score was calculated by using Genetyx ver. 10.0.3 (Genetyx). From 1,514 PB2 sequences from pre-2009 human H1N1 viruses (isolated between 1945 and 2009), 2,278 sequences from avian viruses (isolated after 2010), 103 sequences from human H2N2 viruses, 4,851 sequences from human H3N2 viruses, and 4,469 sequences from human H1N1pdm viruses downloaded from the Influenza Research Database (http://www.fludb.org/brc/home.spg?decorator=influenza), we generated energy-normalized LOGOS plots by using enoLOGOS (31). The height of each represented base was weighted on the basis of its frequency at a position within aligned sequences.

Immunofluorescence assay. The immunofluorescence assay was performed as previously reported (32), with some modifications. Briefly, plasmid-transfected 293 or virus-infected MDCK cells were stained with MitoTracker Green FM (Life Technologies), fixed with 4% paraformal-

dehyde, and then permeabilized with 0.2% Triton X-100. Antigens were probed with the anti-PB2-S1 antibody in Can Get Signal immunostain, solution A (Toyobo), followed by Alexa Fluor 594-conjugated goat anti-rabbit IgG (Life Technologies). Nuclei were stained with Hoechst 33342 (Life Technologies). The cells were then imaged by using a laser scanning microscope (LSM780 system; Carl Zeiss) and analyzed with Zen software (Carl Zeiss).

Subcellular fractionation. Subcellular fractions of plasmid-transfected 293 or virus-infected MDCK cells were prepared by using a detergent-based cell fractionation kit (EzSubcell Fraction kit; Atto) according to the manufacturer's protocol, with detergent. Samples before fractionation (input), cytosolic fractions (cytoplasm), and mitochondrial fractions (mitochondria) were mixed with 2× sample buffer, loaded onto Any kD Mini-Protean TGX precast gels, and then Western blotted with the anti-PB2 antibody clone 21/3, the anti-PB2-S1 antibody, a rabbit anti-phospho-MEK1/2 (Ser217/221) antibody (Cell Signaling Technology), which served as a cytosol marker, and a mouse monoclonal anti-COX IV antibody (clone 20E8C12; Abcam), which served as a mitochondrial marker.

IFN-β promoter reporter assay. 293T cells were transfected with the indicated viral protein expression plasmids (10, 30, 100, and 300 ng), p125-luc (100 ng; kindly provided by T. Fujita, Kyoto University) (33) containing the IFN-β promoter, which drives the expression of firefly luciferase, and pRL-null (50 ng; Promega), which served as a transfection control, with or without a plasmid encoding the constitutively active mutant N-Myc-RIG-IN (50 ng), by using Trans-IT 293. At 24 h posttransfection, firefly and *Renilla* luciferase activities were measured by using the Dual-Glo luciferase assay system (Promega). IFN-β promoter activity was calculated by normalization of the firefly luciferase activity to the *Renilla* luciferase activity. The IFN-β promoter activity without N-Myc-RIG-IN was set to 1. The data are presented as mean relative IFN-β promoter activities ± standard deviations ($n = 3$).

Coimmunoprecipitation assay. The coimmunoprecipitation assay was performed as previously reported (32), with some modifications. Briefly, PB2-S1 was coexpressed with PB2-FLAG, PB1-FLAG, PA-FLAG, or NP-FLAG, and PB1 was coexpressed with PB2-S1-FLAG or PB2-S1 in 293T cells. PB1-FLAG was coexpressed with PB2 and/or PB2-S1 or PB2-S1 Δ1-27 in 293T cells. At 24 h posttransfection, the cells were lysed in lysis buffer (50 mM Tris-HCl [pH 7.4], 150 mM NaCl, 0.5% Nonidet P-40, and Complete Mini protease inhibitor cocktail [Roche]) and incubated for 60 min at 4°C. After clarification by centrifugation, the supernatants were incubated with anti-FLAG M2 magnetic beads (Sigma) or anti-DDDDK-tag pAb-agarose (MBL) overnight at 4°C. A fraction of the supernatant (input) was then mixed with 2× sample buffer and incubated for 5 min at 95°C. After the overnight incubation, the magnetic or agarose beads were washed three times with lysis buffer, suspended in sample buffer, and incubated for 5 min at 95°C. After the beads were removed by centrifugation, the samples were subjected to SDS-PAGE followed by Western blotting with a rabbit anti-FLAG antibody (Sigma), the anti-PB2-S1 antibody, an anti-PB2 antibody (clone 18/1), and a mouse monoclonal anti-PB1 antibody (clone 136/1) (available from our group).

Minigenome assay. A minigenome assay based on the dual-luciferase system was performed as previously reported (34, 35). 293 cells were transfected with viral protein expression plasmids for NP, PA, PB1, and wild-type or mutant PB2 (50 ng each), with a plasmid expressing a reporter vRNA encoding firefly luciferase under the control of the human RNA polymerase I promoter [pPolI-NP (0)Fluc (0); 50 ng], and with pRL-null (50 ng), which expresses *Renilla* luciferase (as a transfection control), with or without a protein expression plasmid for PB2-S1 (2, 6, 20, 60, or 200 ng) or mutant PB2-S1 (60 ng). The luciferase activities in the transfected cells were measured by using the Dual-Glo luciferase assay system at 24 h posttransfection. Polymerase activity was calculated by standardization of the firefly luciferase activity to the *Renilla* luciferase activity. The polymerase activity of wild-type PB2 without PB2-S1 was set to 100%.

Virus growth kinetics in cell culture. After MDCK cells were infected with the indicated viruses at an MOI of 0.001, cell culture supernatants were collected at 6, 12, 24, and 48 h postinfection (hpi) and subjected to virus titration by use of plaque assays with MDCK cells.

Experimental infection of mice. Baseline body weights of 6-week-old female BALB/c mice (Japan SLC) were measured before infection. Under anesthesia, 5 mice per group were intranasally inoculated with 10^2 to 10^6 PFU (50 μl) of the indicated viruses. Body weight and survival were monitored daily for 14 days. Fifty percent mouse lethal dose (MLD_{50}) values were calculated according to the Spearman-Karber method (36, 37). All experiments with mice were performed in accordance with the University of Tokyo's Regulations for Animal Care and Use and were approved by the Animal Experiment Committee of the Institute of Medical Science, the University of Tokyo.

RESULTS

Detection of a spliced mRNA in virus-infected cells. To look for a novel spliced mRNA transcribed from the PB2 segment, we infected 293 cells with WSN at an MOI of 5. At 6 hpi, total RNA extracted from the infected cells was reverse transcribed with an oligo(dT) primer, and PCR was then performed with a series of forward primers, 28F, 200F, 400F, 600F, 800F, 1000F, 1200F, and 1400F, annealing to different sequential positions of the mRNA encoding PB2 (here designated mRNA1), and a reverse primer annealing to the 3′ end of mRNA1. By using this approach, two species of PCR product, a major product and a minor product, were detected on agarose gel electrophoresis (Fig. 1A). We determined the nucleotide sequences of both products by direct sequencing. The nucleotide sequence of the major PCR product was that of mRNA1, and that of the minor PCR product was that of a novel mRNA (here designated mRNA2), which had a deletion corresponding to nucleotides 1513 to 1894 of mRNA1 (Fig. 1B). Around the junction region, we found major consensus sequences for the splice donor (SD) and splice acceptor (SA) sites (underlined in Fig. 1C). mRNA2 encoded a novel, 508-aa viral protein (here designated PB2-S1), which consisted of a 495-aa N-terminal PB2 region and a 13-aa C-terminal PB2-S1-specific region (Fig. 1B). The deletion caused a frameshift and generation of the PB2-S1-specific amino acid region (Fig. 1C). We then evaluated the expression of mRNA1 and mRNA2 in infected MDCK cells by using RT-PCR for the specific detection of mRNA1 and mRNA2. MDCK cells were infected with WSN at an MOI of 10. Total RNA was extracted at 1 to 12 hpi and reverse transcribed with an oligo(dT) primer to obtain cDNA. RT-PCR was performed using 2 sets of primers, specific for mRNA1 and mRNA2. Each primer set specifically amplified cDNA derived from mRNA1 or mRNA2 under the excessive 25 and 35 amplification cycles (Fig. 1D). The mRNA2 expression was first detected at 2 hpi, peaked at 4 to 5 hpi, and remained virtually constant after 7 hpi (Fig. 1E, middle panel). A similar expression pattern was observed for mRNA1 expression (Fig. 1E, upper panel). We estimated that mRNA1 and mRNA2 were expressed at approximately 10^6 to 10^7 and 10^5 to 10^6 copies, respectively, based on the intensities of the PCR products, indicating that approximately 1% of mRNA1 was spliced. These results show that both mRNA2 and mRNA1 are expressed in cells infected with WSN.

Expression of PB2-S1 in virus-infected cells. Because mRNA2 was detected in virus-infected cells, we next assessed whether the PB2-S1 protein was expressed in these cells. MDCK cells were infected with WSN at an MOI of 10. At 1 to 12 hpi, total cell lysates were analyzed by Western blotting with two anti-PB2 monoclonal

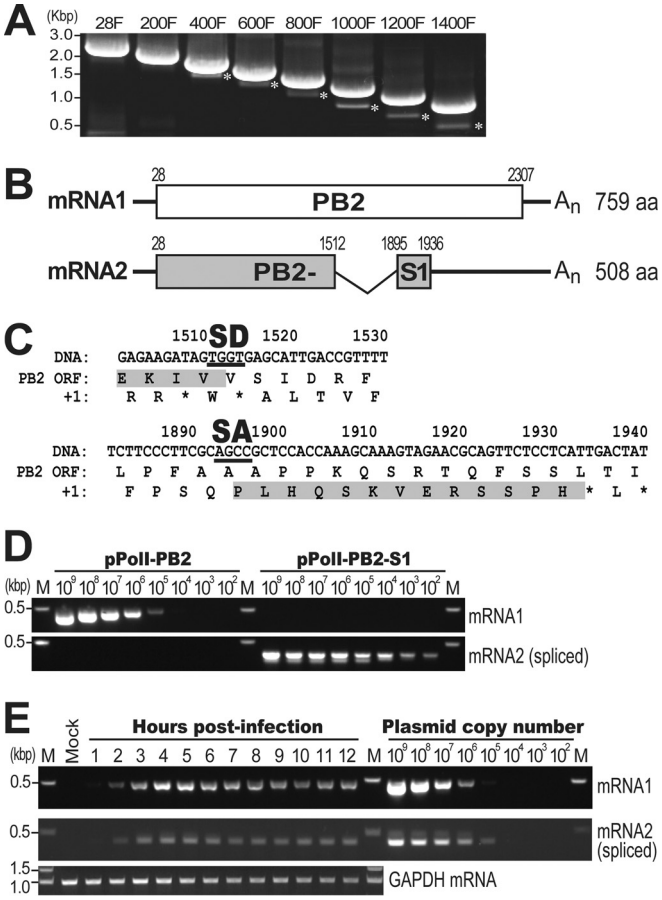

FIG 1 Detection and open reading frame of a novel mRNA from the PB2 segment. (A) Analysis of mRNA expression from the PB2 segment in infected cells. 293 cells were infected with WSN at an MOI of 5. At 6 hpi, total RNA was extracted and reverse transcribed with an oligo(dT) primer. The cDNA from the PB2 gene was amplified by PCR with a series of forward primers that annealed to different positions of mRNA1 and a reverse primer that annealed to the 3′ end of mRNA1. Each asterisk indicates the PCR product of a novel mRNA2. (B) Schematic diagram of an mRNA splice variant from the PB2 segment. The nucleotide coordinates of the splice donor (SD) and splice acceptor (SA) sites are shown for mRNA2. mRNA1 and mRNA2 encode PB2 and PB2-S1, respectively. The total numbers of amino acids are given on the right. (C) Nucleotide sequences (shown as cDNA sequences) and open reading frames (ORFs) around the SD and SA sites of WSN. The nucleotide sequence between the TG at the SD site and the CC at the SA site was deleted in mRNA2. The ORF of PB2-S1 is shaded. (D) Specific detection of mRNA1 and mRNA2 by PCR. PCR was carried out using 2 sets of primers, specific for mRNA1 and mRNA2, and plasmids encoding mRNA1 (pPolI-PB2) and mRNA2 (pPolI-PB2-S1). The number of amplification cycles was 25 for mRNA1 and 35 for mRNA2. Lane M, DNA size marker lane. (E) Detection of mRNA2 in virus-infected cells. MDCK cells were infected with WSN at an MOI of 10. At each indicated time point, total RNA was extracted and reverse transcribed with an oligo(dT) primer. PCR was carried out using 2 sets of primers, specific for mRNA1 and mRNA2. The number of amplification cycles was 20 for mRNA1 and 30 for mRNA2. pPolI-PB2 and pPolI-PB2-S1 were utilized as controls. GAPDH mRNA was amplified as an internal control. Lanes M, DNA size marker lanes.

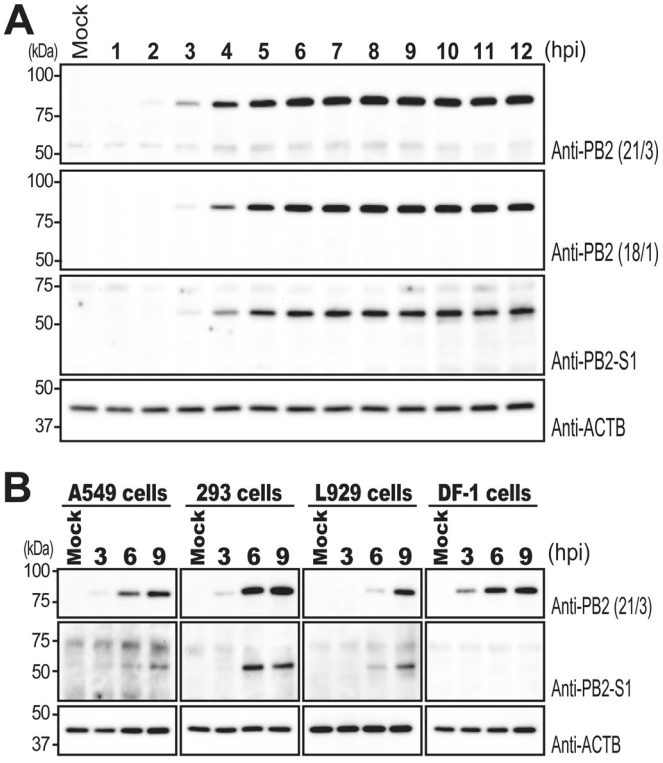

FIG 2 Expression of PB2-S1 in virus-infected cells. (A) Time course analyses of PB2 and PB2-S1 expression. MDCK cells were infected with WSN at an MOI of 10. At each indicated time point, total cell lysates were analyzed by Western blotting with two anti-PB2 monoclonal antibodies (clones 21/3 and 18/1), an anti-PB2-S1 antibody, and an anti-ACTB antibody. (B) PB2-S1 expression in human and mouse cells. Human A549 cells, human 293 cells, mouse L929 cells, and avian DF-1 cells were infected with WSN at an MOI of 10. Total cell lysates were analyzed by Western blotting with the anti-PB2 (clone 21/3), anti-PB2-S1, and anti-ACTB antibodies at 3, 6, and 9 hpi.

antibodies, clones 21/3 and 18/1 (Fig. 2A). Clone 21/3 and clone 18/1 recognize the N- and C-terminal regions of PB2, respectively (30), suggesting that clone 21/3 would detect PB2-S1, whereas clone 18/1 would not. Using these monoclonal antibodies, PB2 was first detected as an approximately 80-kDa band at 3 to 4 hpi, and its expression was maintained until 12 hpi. In the blot probed with clone 21/3, a faint signal was detected at approximately 55 kDa in all lanes, including the mock sample lane, but after 4 hpi, the signal became stronger. To examine whether the 55-kDa band corresponded to PB2-S1, we performed Western blotting with an anti-PB2-S1 antibody that recognizes a specific peptide, PLHQSK VERSSPH, that is present after the splicing junction site in PB2-S1. This anti-PB2-S1 antibody detected a band at approximately 55 kDa after 4 hpi, indicating that PB2-S1 is expressed in virus-infected MDCK cells. Since PB2-S1 was expressed in canine MDCK cells, we next evaluated PB2-S1 expression in human A549 and 293 cells, mouse L929 cells, and avian DF-1 cells (Fig. 2B). These cells were infected with WSN at an MOI of 10, and total cell lysates were analyzed by Western blotting with the anti-PB2 antibody (clone 21/3) and the anti-PB2-S1 antibody at 3, 6, and 9 hpi. PB2 and PB2-S1 were detected in A549, 293, and L929 cells after 3 to 6 hpi. In DF-1 cells, PB2-S1 was not detected, but PB2 was detected after 3 hpi. These results indicate that PB2-S1 is expressed in a host cell-specific manner.

Expression of PB2-S1 in plasmid-transfected cells. M2 or NS2 is produced upon M or NS mRNA expression by a vector because the splicing mechanism is independent of the viral polymerase (38, 39). Therefore, we examined PB2-S1 expression in plasmid-transfected cells. 293 cells were transfected with a plasmid encoding PB2

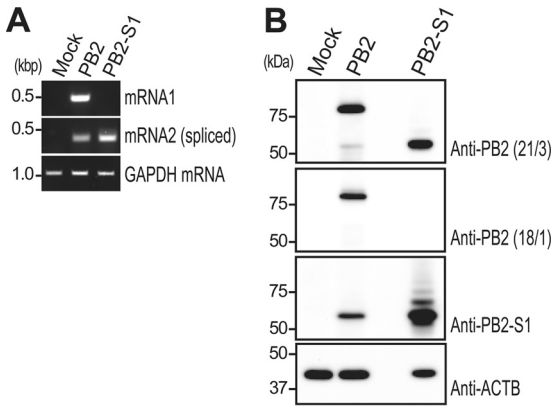

FIG 3 PB2-S1 expression in plasmid-transfected cells. 293 cells were transfected with an empty plasmid (mock) or a plasmid encoding PB2 or PB2-S1. At 24 h posttransfection, total RNA and total cell lysates were prepared. (A) Total RNA was reverse transcribed with an oligo(dT) primer. PCR was performed with 2 sets of primers, specific for mRNA1 and mRNA2. The number of amplification cycles was 18 for mRNA1 and 23 for mRNA2. GAPDH mRNA was amplified as an internal control. (B) Total cell lysates were analyzed by Western blotting with the two anti-PB2 monoclonal antibodies (clones 21/3 and 18/1), the anti-PB2-S1 antibody, and the anti-ACTB antibody.

(mRNA1) or PB2-S1 (mRNA2). At 24 h posttransfection, total RNA was extracted, and RT-PCRs with primers specific for mRNA1 and mRNA2 were performed (Fig. 3A). Both mRNA2 and mRNA1 were detected in cells transfected with the plasmid encoding PB2, whereas mRNA2 but not mRNA1 was detected in cells transfected with the plasmid encoding PB2-S1. In parallel with RT-PCR, total cell lysates were analyzed by Western blotting with the two anti-PB2 monoclonal antibodies, clones 21/3 and 18/1, and the anti-PB2-S1 antibody (Fig. 3B). Clone 21/3 detected a strong signal corresponding to PB2 and a weak signal corresponding to PB2-S1 in cells transfected with a plasmid carrying the entire PB2 coding region, as well as a strong signal corresponding to PB2-S1 in cells transfected with a plasmid encoding PB2-S1. In the case of clone 18/1, PB2 but not PB2-S1 was detected in cells transfected with the PB2-expressing plasmid. Similarly, this antibody did not detect PB2-S1 in cells transfected with the PB2-S1-expressing plasmid, as expected. However, the anti-PB2-S1 antiserum detected PB2-S1 in cells transfected with the plasmid encoding PB2 or PB2-S1; we cannot explain why multiple bands were detected with the anti-PB2-S1 antiserum in the PB2-S1 lane. These results indicate that PB2-S1 and mRNA2 are produced in cells transfected with a plasmid encoding PB2 (mRNA1).

PB2-S1 expression from mRNA1 possessing mutations in the SD and/or SA site. Major consensus sequences have been established for SD and SA sites (26, 40, 41). Substitutions in these consensus sequences abolish the SD and SA sites, resulting in the lack of expression of the spliced mRNA and its encoded protein. To prove that mRNA2 results from splicing, we prepared 5 plasmids encoding PB2 proteins with mutations in the SD and/or SA site (Fig. 4A). PB2 D(CT) and PB2 A(TC) possessed single- and double-nucleotide substitutions in their SD and SA sites, respectively. The G1513C substitution in the D(CT) mutant caused a valine-to-leucine substitution in PB2, at position 496, and the A1893T substitution in the A(TC) mutant caused an alanine-to-proline substitution in PB2, at position 623. PB2 Dsm, PB2 Asm, and PB2 DAsm had several synonymous nucleotide substitutions around the SD site, the SA site, and both sites, respectively. 293 cells were transfected with plasmids carrying the 5 PB2 mutant coding regions and the wild-type PB2 coding region, and Western blotting was performed to assess PB2-S1 expression (Fig. 4B). Under conditions where wild-type and mutant PB2 proteins were detected at similar levels, PB2-S1 was detected in the wild-type PB2 lane but not in any of the mutant PB2 lanes. This result indicates that PB2-S1 is translated from the spliced mRNA2.

Expression of PB2-S1 in cells infected with pre-2009 H1N1 viruses. To assess whether other influenza A viruses express PB2-S1, we selected seven human isolates, including A/Puerto Rico/8/34 (PR8), A/Kawasaki/173/2001 (K173), and A/Gunma/07G006/2008 (Gunma), as representatives of pre-2009 pandemic H1N1 viruses, A/Osaka/164/2009 (Osaka) and A/Yokohama/UT-K2A/2011 (K2A) as representatives of H1N1pdm viruses, and A/Aichi/2/68 (Aichi) and A/Yokohama/UT-K4A/2011 (K4A) as representatives of H3N2 viruses. The PB2 genes of these viruses were sequenced, and splicing scores for their SD and SA sites were calculated by using Genetyx (Fig. 5A): the higher the score, the more likely it is that the site will be spliced. The splicing scores for the SD and SA sites of the three pre-2009 H1N1 isolates were the same or higher than those for WSN, whereas those for the two H1N1pdm isolates were lower than those for WSN. Compared with the scores for WSN, the splicing scores for the two H3N2 isolates were lower for the SD site but similar or higher for the SA site. To examine whether these seven human isolates express PB2-S1, we first attempted to detect the spliced PB2 mRNA2 by RT-PCR. We infected MDCK cells with each of the above-described isolates at an MOI of 10, and total RNA was reverse transcribed with an oligo(dT) primer at 6 hpi. We then performed PCR with

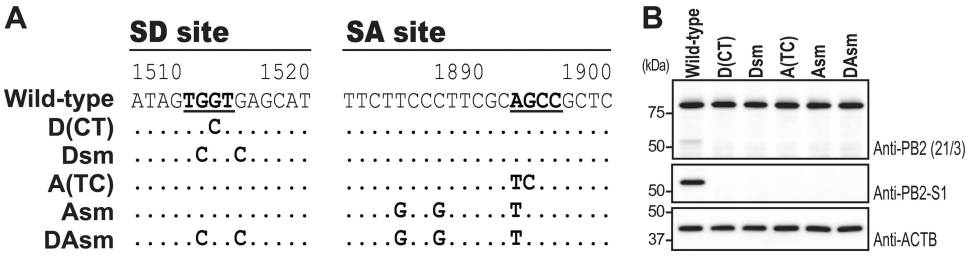

FIG 4 PB2-S1 expression from PB2 possessing mutations in its SD and/or SA site. (A) Nucleotide sequences of PB2 mutants tested for PB2-S1 expression. The SD and SA sites are underlined. The V496L and A623P amino acid mutations are caused by the G1513C substitution in the D(CT) mutant and the A1893T substitution in the A(TC) mutant, respectively. The other nucleotide substitutions did not change the amino acid residues. (B) PB2-S1 expression in plasmid-transfected cells. 293 cells were transfected with plasmids encoding the indicated PB2 proteins. Total cell lysates were analyzed with the anti-PB2 antibody (clone 21/3), the anti-PB2-S1 antibody, and the anti-ACTB antibody.

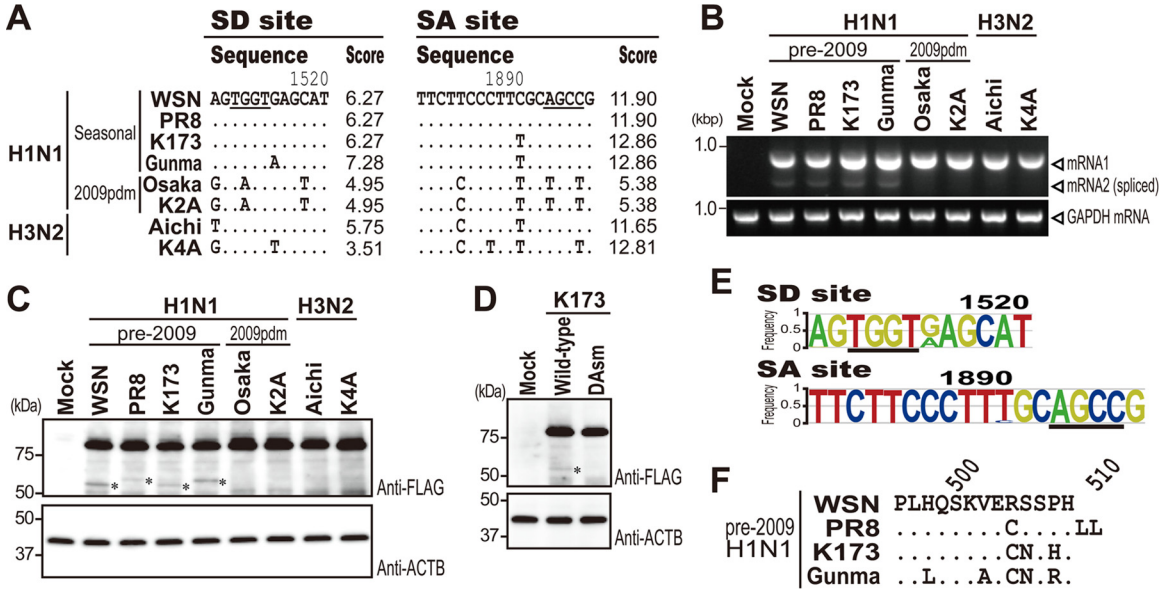

FIG 5 PB2-S1 expression from PB2 derived from 8 human isolates. (A) Comparison of nucleotide sequences around the SD and SA sites of A/Puerto Rico/8/34 (PR8), A/Kawasaki/173/2001 (K173), A/Gunma/07G006/2008 (Gunma), A/Osaka/164/2009 (Osaka), A/Yokohama/UT-K2A/2011 (K2A), A/Aichi/2/68 (Aichi), and A/Yokohama/UT-K4A/2011 (K4A). The SD and SA sites are underlined. The scores denote splicing site scores and represent how similar the splice sites are to the consensus sequence. A high score is indicative of a strong splice site. (B) Expression of PB2 mRNA2 in virus-infected cells. MDCK cells were infected with each indicated isolate at an MOI of 10. At 6 hpi, total RNA was extracted and reverse transcribed with the oligo(dT) primer. The cDNA from the PB2 gene was amplified by PCR with primers uniPB2-1388F and 2307R annealed to PB2 mRNA1. GAPDH mRNA was amplified as an internal control. (C) PB2-S1 expression in plasmid-transfected cells. 293 cells were transfected with a plasmid encoding FLAG-tagged PB2 proteins derived from 8 human isolates. Total cell lysates were analyzed by Western blotting with anti-FLAG and anti-ACTB antibodies. Asterisks indicate the PB2-S1 signal. (D) PB2-S1 expression from K173 wild-type and K173 DAsm mutant PB2. 293 cells were transfected with a plasmid encoding FLAG-tagged wild-type or DAsm mutant PB2. Total cell lysates were analyzed with anti-FLAG and anti-ACTB antibodies. Asterisks indicate the PB2-S1 signal. (E) Energy-normalized sequence logo (enoLOGOS) plots around the SD and SA sites. The height of each represented base is weighted on the basis of its frequency at a given position within the 1,514 PB2 sequences of pre-2009 human H1N1 isolates. The SD and SA sites are underlined. (F) Comparison of PB2-S1-specific amino acid sequences. Amino acid sequences of PB2-S1 proteins, after the splicing junction site, are shown for WSN, PR8, K173, and Gunma.

the primers uniPB2-1388F and PB2-2307R annealed to mRNA1 (Fig. 5B). Both mRNA1 and mRNA2 were detected in WSN-, PR8-, K173-, and Gunma-infected cells, whereas mRNA1 but not mRNA2 was detected in Osaka-, K2A-, Aichi-, and K4A-infected cells. To further test PB2-S1 expression in these seven human isolates, cells were transfected with plasmids encoding PB2 constructs with an N-terminal FLAG tag and then analyzed by Western blotting with an anti-FLAG antibody (Fig. 5C). A protein with a molecular mass similar to that of PB2-S1 was detected in the three pre-2009 H1N1 lanes as well as in the WSN lane (indicated by asterisks), whereas it was not detected in the H1N1pdm or H3N2 lanes. To demonstrate that this protein was indeed PB2-S1 expressed via splicing, we prepared a plasmid encoding the K173 PB2 DAsm mutant, which possessed nucleotide mutations identical to those shown in Fig. 4A. Cells were transfected with a plasmid encoding wild-type K173 PB2 or K173 PB2 DAsm, and total cell lysates were analyzed by Western blotting with the anti-FLAG antibody at 24 h posttransfection (Fig. 5D). A band with a molecular mass similar to that of PB2-S1 was detected in the wild-type K173 PB2 lane but not in the K173 PB2 DAsm lane, suggesting that the band with a molecular mass similar to that of PB2-S1 was indeed PB2-S1 produced by splicing and that not only WSN but also pre-2009 H1N1 PB2 expresses PB2-S1.

To further confirm that PB2-S1 is expressed in most pre-2009 H1N1 isolates, the nucleotide sequences around the SD and SA sites of 1,514 pre-2009 H1N1 PB2 sequences deposited in the Influenza Research Database were analyzed by using enoLOGOS (Fig. 5E). Two major sites of diversity were found: G or A at position 1515, around the SD site, and T or C at position 1890, around the SA site. These variations were also found in the isolates used in this study (Fig. 5A) and did not affect PB2-S1 expression. Our results show that PB2-S1 is conserved among pre-2009 H1N1 influenza viruses. To assess the function of PB2-S1, we compared the PB2-S1-specific amino acid sequences among four isolates tested here (Fig. 5F). Even among these four isolates, we found variations in the sequence and length of the PB2-S1-specific amino acid region. These PB2-S1-specific amino acid sequences were analyzed by using the PROSITE program (http://prosite.expasy.org/) to identify functional motifs; however, no functional sequence motifs were identified. These findings may suggest that PB2-S1 functions as a C-terminally deleted PB2 protein rather than via its specific amino acid sequence.

PB2-S1 localizes to mitochondria via its N-terminal mitochondrial localization signal. Although most PB2 localizes to the nucleus via its nuclear localization signal, where it functions in the viral polymerase complex with PA and PB1 (42), a portion of PB2 localizes to mitochondria via its N-terminal mitochondrial localization signal (43, 44). To understand PB2-S1 functions, we first determined the intracellular localization of PB2-S1 after plasmid transfection. 293 cells were transfected with empty plasmid or pCA-PB2-S1. These cells were then stained with the anti-PB2-S1 antibody and MitoTracker at 24 h posttransfection (Fig. 6A).

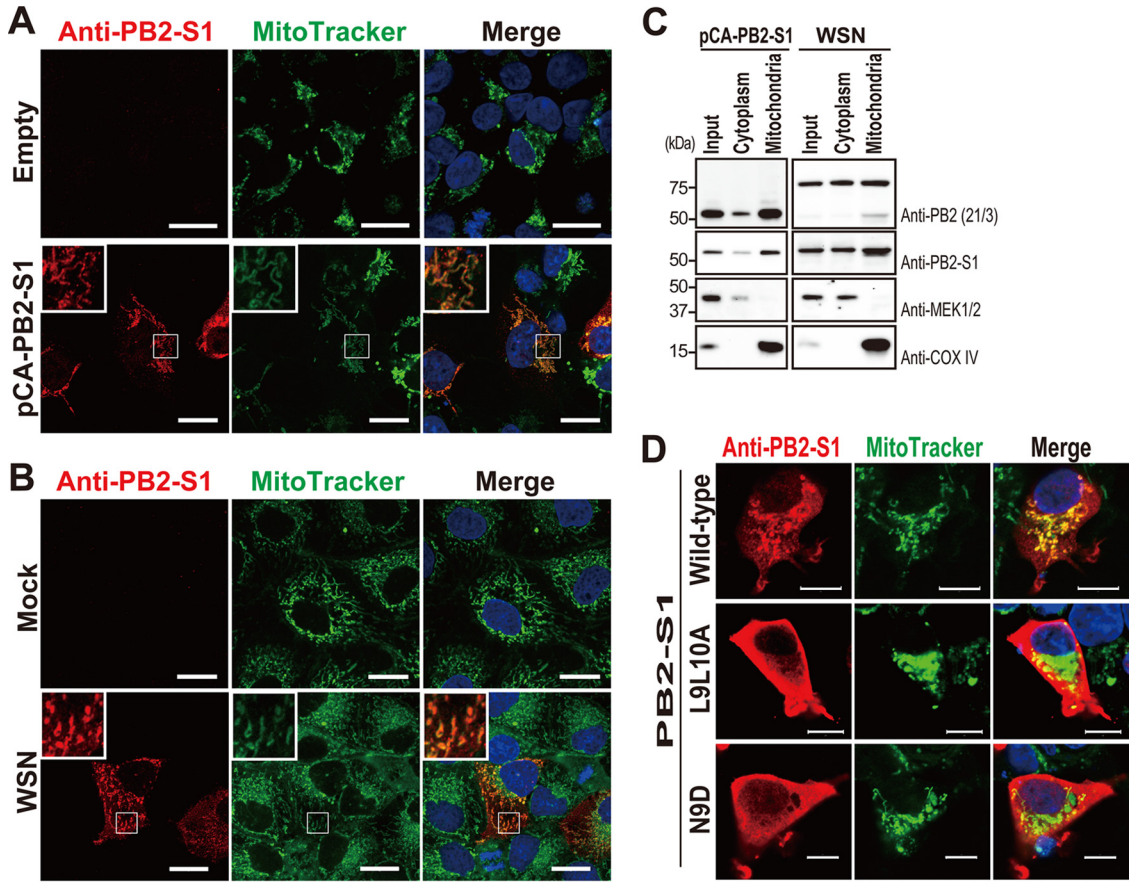

FIG 6 PB2-S1 localizes to mitochondria via its N-terminal mitochondrial localization signal. (A and B) Microscopic analyses of the intracellular localization of PB2-S1. 293 cells were transfected with empty plasmid (empty) or the plasmid encoding PB2-S1 (pCA-PB2-S1) (A), and MDCK cells were mock infected (mock) or infected with WSN at an MOI of 0.1 (WSN) (B). At 24 h posttransfection and 6 hpi, the cells were stained with the anti-PB2-S1 antibody (red) and MitoTracker (green). Nuclei were stained with Hoechst 33342 (blue). Insets show higher-magnification views of the indicated portions of the cells. Bars, 20 μm. (C) Analysis of the intracellular localization of PB2-S1 by means of subcellular fractionation. 293 cells were transfected with the plasmid encoding PB2-S1 (pCA-PB2-S1), and MDCK cells were infected with WSN at an MOI of 10 (WSN). At 24 h posttransfection and 9 hpi, cell lysates (input) were fractionated into cytosolic (cytoplasm) and mitochondrial (mitochondria) fractions and then analyzed by Western blotting with the anti-PB2 antibody (clone 21/3), the anti-PB2-S1 antibody, an anti-MEK1/2 antibody (cytosol), or an anti-COX IV antibody (mitochondria). (D) Intracellular localization of mutant PB2-S1. 293 cells were transfected with the plasmid encoding wild-type PB2-S1, PB2-S1 L7L10A, or PB2-S1 N9D. The cells were stained with the anti-PB2-S1 antibody (red), MitoTracker (green), and Hoechst 33342 (blue) at 24 h posttransfection. Bars, 10 μm.

PB2-S1 was mainly detected in the cytoplasm and colocalized with mitochondria. A weak PB2-S1 signal was also observed in the nucleus. We observed no nonspecific staining with the anti-PB2-S1 antibody in cells transfected with empty plasmid. We next examined the localization of PB2-S1 in virus-infected cells (Fig. 6B). MDCK cells were mock infected or infected with WSN at an MOI of 0.1 and were then stained with the anti-PB2-S1 antibody and MitoTracker at 6 hpi. Similar to our findings after plasmid transfection, PB2-S1 in virus-infected cells colocalized with mitochondria in the cytoplasm, and no nonspecific staining with the anti-PB2-S1 antibody was observed in the mock-infected cells. To confirm these microscopic observations, plasmid-transfected or virus-infected cells were subjected to subcellular fractionation to obtain cytoplasmic and mitochondrial fractions (Fig. 6C). Under conditions where phosphorylated MEK1/2 served as a cytoplasmic fraction marker and COX IV served as a mitochondrial marker, the mitochondrial fractions from plasmid-transfected and virus-infected cells contained PB2-S1. These results show that a portion of PB2-S1 localizes to mitochondria.

The mitochondrial localization signal of authentic PB2 is abolished by the amino acid substitution N9D (PB2 N9D) or by the double substitutions L7A/L10A (PB2 L7L10A) (43, 44). Therefore, we prepared mutant PB2-S1 proteins possessing these amino acid changes and examined the intracellular localization of these mutants. When 293 cells were transfected with plasmids encoding wild-type PB2-S1, PB2-S1 L7L10A, or PB2-S1 N9D and were stained with the anti-PB2-S1 antibody and MitoTracker (Fig. 6D), wild-type PB2-S1 was detected in the cytoplasm and found to localize to mitochondria. Both PB2-S1 mutants were diffusely detected in the cytoplasm and did not localize to mitochondria, indicating that PB2-S1 utilizes a mitochondrial localization signal identical to that of authentic PB2 for mitochondrial localization.

PB2-S1 inhibits the RIG-I-dependent IFN signaling pathway. PB2 inhibits RIG-I-mediated IFN-β expression by binding to the mitochondrial antiviral signaling protein (MAVS) (43, 45). Therefore, we asked whether PB2-S1 could inhibit the RIG-I-dependent IFN signaling pathway. pCA-N-Myc-RIG-IN, which en-

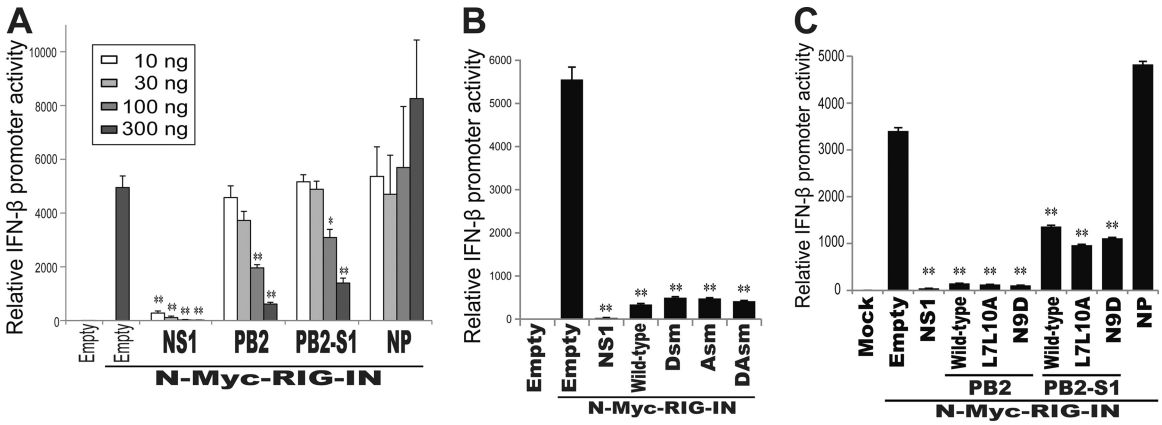

FIG 7 PB2-S1 interferes with the RIG-I-dependent IFN signaling pathway. (A) Inhibition of the RIG-I-dependent IFN signaling pathway by PB2-S1. 293T cells were transfected with the indicated viral protein expression plasmids, p125-luc, and pRL-null, with or without a plasmid encoding the constitutively active mutant N-Myc-RIG-IN. Firefly and *Renilla* luciferase activities were measured by means of a dual-luciferase assay. IFN-β promoter activity was calculated by normalization of the firefly luciferase activity to the *Renilla* luciferase activity. The IFN-β promoter activity without N-Myc-RIG-IN was set to 1. The data are shown as mean relative IFN-β promoter activities ± standard deviations ($n = 3$). * and **, $P < 0.05$ and $P < 0.01$, respectively (one-way analysis of variance [ANOVA] followed by Dunnett's test). (B and C) Inhibition of the RIG-I-dependent IFN signaling pathway by PB2-S1-deficient PB2 and mitochondrial localization-deficient PB2-S1. IFN-β promoter assays were performed using plasmids encoding PB2-S1-deficient PB2 and mitochondrial localization-deficient PB2 or PB2-S1. The data are shown as the mean relative IFN-β promoter activities ± standard deviations ($n = 3$). **, $P < 0.01$ (one-way ANOVA followed by Dunnett's test).

codes a constitutively active mutant of human RIG-I, and p125-luc, which contains the IFN-β promoter driving the expression of firefly luciferase, were used for activation and quantification of the IFN-β promoter activity (33, 46). These plasmids, together with an empty plasmid, pCA-NS1, pCA-PB2, pCA-PB2-S1, or pCA-NP and pRL-null, as a transfection control, were transfected into 293T cells, and luciferase activities were measured at 24 h posttransfection (Fig. 7A). The activation of the IFN-β promoter by N-Myc-RIG-IN was inhibited by either NS1 or PB2 expression in a dose-dependent manner, as reported previously (43, 45, 47, 48). The activation was also inhibited by PB2-S1 expression, to an extent similar to that achieved with PB2; however, activation of the IFN-β promoter was not inhibited by NP expression. These data show that PB2-S1 interferes with the RIG-I-dependent IFN signaling pathway.

To examine whether the inhibitory effect was shared by authentic PB2 and PB2-S1, an IFN-β promoter assay was performed with plasmids encoding wild-type PB2, PB2 Dsm, PB2 Asm, and PB2 DAsm (Fig. 7B). All three PB2-S1-deficient PB2 mutants inhibited the activation of the IFN-β promoter via N-Myc-RIG-IN, to an extent similar to that for wild-type PB2. These data show that PB2 and PB2-S1 independently possess inhibitory effects on the RIG-I-dependent IFN signaling pathway.

We next evaluated the inhibition of the RIG-I-dependent pathway by mitochondrial localization-deficient PB2-S1 and PB2. The IFN-β promoter assay was performed with plasmids encoding PB2 or PB2-S1 possessing the L7L10A or N9D amino acid substitution (Fig. 7C). Again, influenza viral NS1 inhibited the RIG-I-dependent signaling pathway, but viral NP did not. PB2 L7L10, PB2 N9D, PB2-S1 L7L10A, and PB2-S1 N9D exhibited inhibitory effects on the RIG-I-dependent pathway similar to those of wild-type PB2. These results suggest that the mitochondrial localization of PB2-S1 and PB2 is not required for inhibition of the RIG-I-dependent signaling pathway.

Obstruction of viral polymerase activity by PB2-S1 is dependent on its PB1-binding capability. PB2 interacts with PB1, PA, and NP (49–52). To examine whether PB2-S1 also binds to these viral proteins, we performed a coimmunoprecipitation assay. PB2-S1 was coexpressed with PB2-FLAG, PB1-FLAG, PA-FLAG, and NP-FLAG from plasmids or was mock cotransfected into 293T cells, and an immunoprecipitation (IP) assay with an anti-FLAG-tag antibody was performed (Fig. 8A). The levels of PB2, PB1, PA, and NP in the input were varied, whereas PB2-S1 was detected at similar levels in all input lanes (Fig. 8A, left panels). In the IP samples, PB2-S1 was detected in the PB1 lane but not in the mock, PB2, PA, or NP lane (Fig. 8A, right panels). A similar observation was made for the reverse experiments, i.e., immunoprecipitation of C-terminally FLAG-tagged PB2-S1 (PB2-S1-FLAG) by using a rabbit anti-FLAG antibody and detection of coimmunoprecipitated PB1 by using an anti-PB1 monoclonal antibody (Fig. 8B). These results show that PB2-S1 binds to PB1, although the possibility that PB2-S1 interacts with other viral proteins in virus-infected cells cannot be ruled out.

To assess whether PB2-S1 inhibits viral polymerase activity via PB1 binding, we conducted a minigenome assay with PB2-S1. 293 cells were transfected with plasmids encoding NP, PA, PB1, and PB2; with pPolI-NP (0)Fluc (0), which expresses a reporter vRNA encoding firefly luciferase under the control of the human RNA polymerase I promoter; with pRL-null as a transfection control; and with various amounts of the plasmid encoding wild-type PB2-S1. Viral polymerase activity was calculated by standardization of the firefly luciferase activity to the *Renilla* luciferase activity. The viral polymerase activity was inhibited in the presence of PB2-S1, in a dose-dependent manner (Fig. 8C). Under conditions of overexpression (200 ng of pCA-PB2-S1), the viral polymerase activity was reduced to 40% of that without PB2-S1. To confirm that PB2-S1 interfered with the viral polymerase activity via its interaction with PB1, we utilized PB2-S1 mutants that lacked the ability to bind to PB1. A leucine-to-aspartic acid substitution at position 7 (L7D) or deletion of the N-terminal 12 or 27 residues (Δ1-12 or Δ1-27) in PB2 abolishes its ability to bind to PB1 (49, 53); therefore, we prepared PB2-S1 L7D, PB2-S1 Δ1-12, and PB2-S1 Δ1-27.

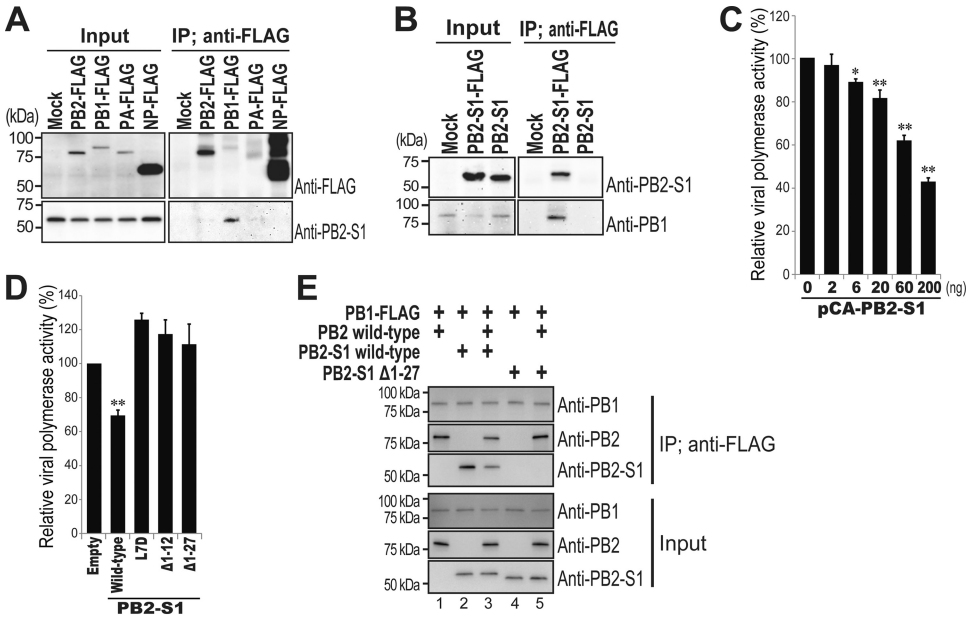

FIG 8 PB2-S1 interacts with PB1 and disrupts viral polymerase activity. (A and B) Interaction of PB2-S1 with PB1. PB2-S1 was coexpressed with PB2-FLAG, PB1-FLAG, PA-FLAG, or NP-FLAG in 293T cells (A), or PB1 was coexpressed with PB2-S1-FLAG or PB2-S1 in 293T cells (B). After immunoprecipitation with an anti-FLAG antibody, the precipitated proteins were analyzed by Western blotting with an anti-FLAG antibody, the anti-PB2-S1 antibody, and an anti-PB1 antibody. Input and IP, total cell lysates and immunoprecipitated samples, respectively. (C and D) PB2-S1 inhibited viral polymerase activity by interacting with PB1. 293 cells were transfected with plasmids encoding PB2, PB1, PA, and NP (50 ng each), with a plasmid encoding wild-type (C) or mutant (D) PB2-S1, with pPolI-NP (0)Fluc (0), and with pRL-null. Firefly and *Renilla* luciferase activities were measured by means of a dual-luciferase assay. Polymerase activity was calculated by normalization of the firefly luciferase activity to the *Renilla* luciferase activity. The polymerase activity without PB2-S1 was set to 100%. The data are shown as mean relative polymerase activities ± standard deviations ($n = 3$). * and **, $P < 0.05$ and $P < 0.01$, respectively (one-way ANOVA followed by Dunnett's test). (E) Competitive binding of PB2 and PB2-S1 to PB1. PB1-FLAG was coexpressed with the indicated combination of PB2 and/or PB2-S1 or its mutant in 293T cells. After immunoprecipitation with the anti-FLAG antibody, the precipitated proteins were analyzed by Western blotting with the anti-PB2 antibody (clone 18/1), the anti-PB2-S1 antibody, and the anti-PB1 antibody. Input and IP, total cell lysates and immunoprecipitated samples, respectively.

We confirmed that these three PB2-S1 mutants did not interact with PB1 by using a coimmunoprecipitation assay (data not shown). We also used these PB2-S1 mutants in the minigenome assay (Fig. 8D). Wild-type PB2-S1 inhibited the viral polymerase activity, whereas all three PB2-S1 mutants did not. These results suggest that PB2-S1 interferes with the viral polymerase activity by binding to PB1.

Next, we tried to directly demonstrate that PB2-S1 competes with PB2 for binding to PB1. PB1-FLAG was coexpressed in 293T cells with the indicated combinations of PB2, wild-type PB2-S1, and PB2-S1 Δ1-27. After immunoprecipitation with the anti-FLAG antibody, the precipitated proteins were analyzed by Western blotting with the anti-PB2 antibody (clone 18/1), the anti-PB2-S1 antibody, and the anti-PB1 antibody (clone 136/1) (Fig. 8E). PB2 and wild-type PB2-S1 each coprecipitated with PB1-FLAG (lanes 1 and 2), but PB2-S1 Δ1-27 did not (lane 4). When both PB2 and wild-type PB2-S1 were expressed together, the amounts of each protein coimmunoprecipitated with PB1-FLAG (lane 3) were smaller than those expressed when each protein was expressed alone (lanes 1 and 2). PB2-S1 Δ1-27 did not affect the amount of PB2 coprecipitated with PB1-FLAG (lane 5). These results indicate that PB2-S1 competes with PB2 for binding to PB1.

Characterization of PB2-S1-deficient viruses. Finally, to characterize the function of PB2-S1 in the virus replication cycle, we prepared PB2-S1-deficient viruses and compared their properties with those of wild-type virus. As described above, some nucleotide mutations within the PB2 sequence abolished PB2-S1 expression (Fig. 4). To test whether these nucleotide mutations affected PB2 functions, especially the viral polymerase activity, we performed the minigenome assay with wild-type PB2, PB2 D(CT), PB2 Dsm, PB2 A(TC), PB2 Asm, and PB2 DAsm (Fig. 9A). PB2 Dsm, PB2 Asm, and PB2 DAsm showed viral polymerase activities similar to that of wild-type PB2, whereas PB2 D(CT) and PB2 A(TC) showed reduced activities. These results indicate that the substitutions in PB2 D(CT) and PB2 A(TC) affect the function of PB2 as a subunit of the viral polymerase. These results also suggest that PB2-S1 deficiency does not affect the viral polymerase activity. We generated mutant WSN viruses possessing genes for PB2 Dsm, PB2 Asm, and PB2 DAsm in the genome and then confirmed PB2-S1 expression by infecting MDCK cells with these mutant viruses at an MOI of 10, followed by Western blotting with the anti-PB2 antibody clone 21/3 and the anti-PB2-S1 antibody (Fig. 9B). Under conditions where each PB2 protein was detected at a similar level, PB2-S1 was detected in wild-type virus-infected cells but not in PB2 Dsm, PB2 Asm, or PB2 DAsm virus-infected cells, indicating that PB2-S1 is translated from the spliced mRNA in virus-infected cells. These mutant viruses were then evaluated for their growth efficiency in MDCK cells at a low MOI, and they showed growth kinetics similar to those of wild-type virus (Fig. 9C). Next, we compared the viral pathogenicities of different doses of the wild-type and mutant viruses in mice (Fig. 9D). The three mutant viruses showed pathogenicities almost identical to that of wild-

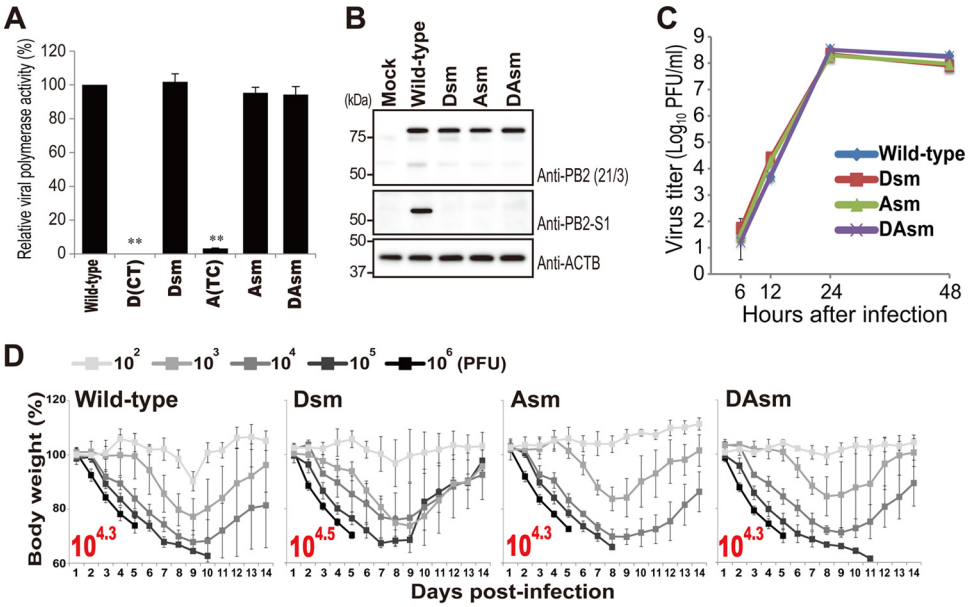

FIG 9 Properties of PB2-S1-deficient viruses. (A) Viral polymerase activity of PB2-S1-deficient PB2. 293 cells were transfected with plasmids encoding PB1, PA, NP, and wild-type or mutant PB2, with pPolI-NP (0)Fluc (0), and with pRL-null. Polymerase activity was calculated as described in the legend to Fig. 8. The data are shown as mean relative polymerase activities ± standard deviations ($n = 3$). **, $P < 0.01$ (one-way ANOVA followed by Dunnett's test). (B) PB2-S1 expression in cells infected with viruses possessing SD and/or SA site mutations in PB2. MDCK cells were infected with the indicated mutant viruses at an MOI of 10. At 9 hpi, total cell lysates were analyzed by Western blotting with the anti-PB2 antibody (clone 21/3), the anti-PB2-S1 antibody, and the anti-ACTB antibody. (C) Viral growth kinetics of PB2-S1-deficient viruses in MDCK cells. MDCK cells were infected with the indicated viruses at an MOI of 0.001. At each indicated time point, virus titers were determined by means of plaque assays. The data are shown as mean virus titers ± standard deviations ($n = 3$). (D) Virulence of mutant viruses in mice. Five mice per group were inoculated intranasally with 10^2, 10^3, 10^4, 10^5, or 10^6 PFU (each in 50 μl) of the indicated viruses. Body weight and survival were monitored daily for 14 days. The values represent average body weights compared to baseline weights ± standard deviations for five mice. MLD_{50} values (shown in red) were calculated according to the Spearman-Karber method.

type virus, with MLD_{50} values for the wild-type, PB2 Dsm, PB2 Asm, and PB2 DAsm viruses of $10^{4.3}$, $10^{4.5}$, $10^{4.3}$, and $10^{4.3}$, respectively. These data imply that PB2-S1 is not essential for WSN virus replication in MDCK cells or for its pathogenicity in mice.

DISCUSSION

In the present study, we identified the novel viral protein PB2-S1, which is translated from spliced mRNA transcribed from the PB2 segment. Among the alternative viral proteins, M2, M42, NS2, and NS3 are translated from spliced mRNA (5–16), PB1-F2, PB1-N40, PA-N155, and PA-N182 are expressed via an alternative translation initiation process (17–21), and PA-X is expressed via a ribosomal frameshift (25). PB2-S1 is the second viral protein expressed from the PB2 segment and is the fifth viral protein translated from a spliced mRNA. Since splicing plays an essential role in host gene expression via the removal of intron sequences from pre-mRNA, major consensus motifs for splice donor (SD) and splice acceptor (SA) sites in the human genome have been well characterized (26), allowing us to speculate, on the basis of a calculated splicing site score, whether a viral mRNA might be edited by splicing. The splicing site score expresses how similar the splice site is to the consensus motif; a high score is indicative of a strong splice site candidate. The splicing site scores for PB2-S1 were 6.27 (SD site) and 11.90 (SA site) for the PB2 segment of WSN, whereas the scores for M2 and NS2 were 7.03 (SD site for M2), 5.77 (SA site for M2), 5.78 (SD site for NS2), and 12.28 (SA site for NS2) for the M and NS segments of WSN. Given the high splicing scores for PB2-S1, it is not surprising that the mRNA encoding PB2 is spliced at these sites.

When we assumed that a splicing site score of >5 was indicative of a splicing site, we found that the PB1 segment of WSN had 6 putative SD and 3 putative SA sites, the PA segment had 6 putative SD and 9 putative SA sites, the HA segment had 5 putative SD and 4 putative SA sites, the NP segment had 7 putative SD and 6 putative SA sites, and the NA segment had no putative sites. These findings suggest that other, as yet unidentified novel viral proteins, in addition to PB2-S1, might be expressed from spliced mRNAs transcribed from the PB1, PA, HA, and NP segments of WSN. However, splicing sites cannot be assigned merely on the basis of splicing site scores, because we do not really know how the cellular splicing machinery is regulated during the selection of splicing sites (26). Furthermore, splicing during a viral infection is modulated by viral proteins, such as NS1 (27, 54). Therefore, further studies are needed to confirm whether other novel viral proteins, some of which might not be functional, are expressed from these deduced spliced mRNAs. Although further analyses are needed to confirm the existence of these novel deduced spliced mRNAs, we can assume that a variety of splice products derived from viral RNA exist in virus-infected cells. Identification and characterization of novel viral proteins translated from spliced mRNA could provide new insights into the replication and pathogenicity of influenza virus.

PB2-S1 localized to mitochondria in plasmid-transfected and virus-infected cells and inhibited the RIG-I-dependent IFN signaling pathway. Since the N-terminal 495 amino acids of PB2-S1

are identical to those of PB2, PB2-S1 has a mitochondrial localization signal at positions 1 to 120 (44) and a nuclear localization signal at positions 449 to 495 (42). We found that the intracellular localization of PB2-S1 was defined mainly by the N-terminal mitochondrial localization signal. An active role for the nuclear localization signal within PB2-S1 was not clarified by the cellular distribution of PB2-S1. One group reported that the mitochondrial localization, but not MAVS binding, of PB2 contributes to the inhibition of the RIG-I-dependent pathway (43). However, another group reported that the MAVS binding, but not mitochondrial localization, of PB2 is associated with the inhibition of RIG-I-dependent signaling (45). Therefore, the relationship between mitochondrial localization and MAVS binding with respect to PB2-induced inhibition of the RIG-I-dependent pathway has been unclear. In the present study, we clarified this relationship by showing that mitochondrial localization of PB2-S1 and PB2 is not required to inhibit the RIG-I-dependent signaling pathway. Our results suggest that the binding of PB2 or PB2-S1 to MAVS is essential for the inhibition and that, to inhibit the RIG-I-dependent IFN signaling pathway, PB2-S1 binds to MAVS via amino acids 120 to 242, which represent the most important region in PB2 for MAVS binding (45). Although PB2-S1 inhibited the RIG-I-dependent signaling pathway *in vitro*, PB2-S1 deficiency had no effect on viral growth kinetics in cultured cells or on virus pathogenicity in mice. These findings suggest that PB2-S1 functions as an inhibitory factor for RIG-I-dependent IFN signaling during infection in animals other than mice or that NS1, which exhibits strong inhibitory effects on innate immune responses, masks the effects of PB2-S1 during infection. Further analyses are needed to fully characterize the inhibitory effect of PB2-S1 on the RIG-I-dependent IFN signaling pathway.

PB2-S1 interacted with PB1 in plasmid-transfected cells. PB2 interacts with PB1, PA, and NP (51, 52, 55) during viral genome replication. PB2 has three PB1-binding sites and two NP-binding sites, at amino acid positions 1 to 130 (49, 50, 53), 206 to 259 (56), and 580 to 759 (50) and amino acid positions 1 to 269 and 580 to 683 (50), respectively. No PA-binding sites on PB2 have yet been reported. Therefore, PB2-S1, which has the N-terminal 495 amino acids of PB2, contains two PB1-binding sites and an NP-binding site. We found that PB2-S1 interacts with PB1 and that this interaction was abolished by the L7D substitution or by deletion of the N-terminal 12 or 27 amino acids of PB2-S1. These results demonstrate that the major PB1-binding site of PB2-S1 maps to amino acid positions 1 to 130, particularly the 12 N-terminal amino acids (53). Binding of PB2-S1 to PB1 led to the suppression of viral polymerase activity, suggesting that PB2-S1 and PB2 bind competitively to PB1. The functional viral polymerase consists of a heterotrimeric complex of PB1, PB2, and PA (57, 58). Two different processes have been proposed for the assembly of this trimeric PB2-PB1-PA complex: (i) a PB1-PA dimer forms in the cytoplasm and is transported into the nucleus, where it binds to PB2 (59); or (ii) a PB2-PB1 dimer forms in the cytoplasm and is transported into the nucleus, where it interacts with PA (60). In the former case, PB2-S1 and PB2 would competitively interact with the PB1-PA dimer in the nucleus, whereas in the latter case PB2-S1 and PB2 would competitively interact with free PB1 in the cytoplasm. We confirmed that PB2-S1 competes with PB2 for binding to PB1, supporting the idea that PB2-S1 interacts with PB1. In either case, such competition would appear as inhibitory activity in the viral minigenome assay. However, PB2-S1-deficient PB2 mutants showed polymerase activities identical to that of wild-type PB2, and PB2-S1-deficient viruses grew as efficiently as wild-type virus in cell culture. Therefore, the suppression of viral polymerase activity by PB2-S1 via PB1 binding requires further analysis.

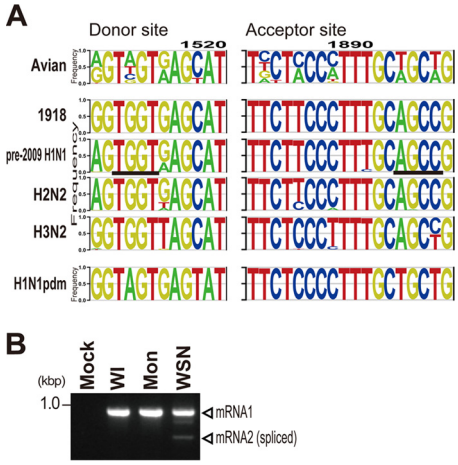

FIG 10 Conservation of the SD and SA sites of PB2. (A) enoLOGOS plots around the SD and SA sites. The height of each represented base is weighted on the basis of its frequency at a given position within 1,514 PB2 sequences of pre-2009 human H1N1 isolates, 2,278 PB2 sequences of avian viruses (isolated after 2010), 103 PB2 sequences of human H2N2 viruses, 4,851 PB2 sequences of human H3N2 viruses, and 4,469 PB2 sequences of human H1N1pdm viruses. 1918, A/Brevig Mission/1/18. The SD and SA sites in pre-2009 H1N1 viruses are underlined. (B) Expression of PB2 mRNA2 in avian influenza virus-infected cells. MDCK cells were infected with A/duck/Wisconsin/8/74 (H3N2; WI) or A/duck/Mongolia/301/2001 (H3N2; Mon) at an MOI of 10. At 6 hpi, RT-PCR was performed with primers uniPB2-1388F and 2307R annealed to PB2 mRNA1. WSN served as a positive control.

PB2-S1 was expressed in cells infected with each of the four pre-2009 pandemic H1N1 isolates we tested, yet H1N1pdm and H3N2 isolates did not express PB2-S1. The PB2 segment of pre-2009 H1N1 viruses, H2N2 viruses, and H3N2 viruses originated from the 1918 virus, which is thought to have derived from an avian virus (61, 62), whereas that of H1N1pdm viruses originated from a North American avian virus (63). Therefore, we examined the conservation of the SD and SA sites for PB2-S1 expression identified in pre-2009 H1N1 viruses in 2,278 avian isolates, A/Brevig Mission/1/18 (H1N1) (1918), 103 human H2N2 isolates, 4,854 human H3N2 isolates, and 4,475 post-2009 human H1N1 isolates (H1N1pdm) (Fig. 10A). Similar to the high conservation among pre-2009 H1N1 isolates (Fig. 5E), the nucleotide sequences of the SD and SA sites are highly conserved among the members of each group except for avian isolates. Compared with that of the 1918 virus, the PB2 segment of H3N2 isolates differs by three nucleotides, including a G1515T substitution around the SD site and T1884C and C1887T substitutions around the SA site, whereas the PB2 segment of pre-2009 H1N1 and H2N2 isolates differs by only one nucleotide, namely, a G1509A substitution near the SD site. Based on the nucleotide sequences of SD and SA sites, the 1918 virus and H2N2 isolates likely express PB2-S1. The avian isolates tested did not express spliced PB2 mRNA2 in MDCK cells (Fig. 10B), and WSN virus did not express PB2-S1 in avian cells. Taken together, these findings suggest that PB2-S1 may be positively maintained during circulation in humans and that H3N2 isolates might encode a viral accessory protein func-

tionally similar to PB2-S1. Further studies are required to fully explore this possibility.

In summary, we identified the novel viral protein PB2-S1, which is encoded by a spliced mRNA derived from the PB2 segment. This novel viral protein appears to be conserved among pre-2009 human pandemic H1N1 viruses, binds to PB1, localizes to mitochondria, and inhibits the RIG-I-dependent signaling pathway. The identification of PB2-S1 suggests that other, as yet unidentified viral proteins encoded by spliced mRNAs could be present in virus-infected cells. Further studies on viral spliced mRNAs, namely, a viral spliceosome, could provide novel insights into viral replication.

ACKNOWLEDGMENTS

We thank Ryuta Uraki, Yuki Usui, and Hiroki Ui for assistance with experiments, Takashi Fujita for providing p125-luc, and Susan Watson for editing the manuscript.

This work was supported by a Grant-in-Aid for Scientific Research (C) (grant 26460549) from the Japan Society for the Promotion of Science; by the Japan Initiative for Global Research Network on Infectious Diseases (J-GRID) from the Ministry of Education, Culture, Sports, Science, and Technology, Japan, and the Japan Agency for Medical Research and Development, AMED; by grants-in-aid from the Ministry of Health, Labor, and Welfare, Japan; by ERATO (Japan Science and Technology Agency); by Strategic Basic Research Programs of the Japan Science and Technology Agency; and by an NIH Functional Genomics award for "characterization of novel genes encoded by RNA and DNA viruses" (grant U19 AI 107810).

FUNDING INFORMATION

Japan Agency for Medical Research and Development, AMED provided funding to Yoshihiro Kawaoka. NIH provided funding to Yoshihiro Kawaoka. Ministry of Education, Culture, Sports, Science, and Technology (MEXT) provided funding to Yoshihiro Kawaoka. Japan Society for the Promotion of Science (JSPS) provided funding to Seiya Yamayoshi under grant number 26460549. Japan Science and Technology Agency (JST) provided funding to Yoshihiro Kawaoka. Ministry of Health, Labour and Welfare (MHLW) provided funding to Yoshihiro Kawaoka.

REFERENCES

1. **McGeoch D, Fellner P, Newton C.** 1976. Influenza virus genome consists of eight distinct RNA species. Proc Natl Acad Sci U S A **73:**3045–3049. http://dx.doi.org/10.1073/pnas.73.9.3045.
2. **Palese P, Schulman JL.** 1976. Mapping of the influenza virus genome: identification of the hemagglutinin and the neuraminidase genes. Proc Natl Acad Sci U S A **73:**2142–2146. http://dx.doi.org/10.1073/pnas.73.6.2142.
3. **Ritchey MB, Palese P, Schulman JL.** 1976. Mapping of the influenza virus genome. III. Identification of genes coding for nucleoprotein, membrane protein, and nonstructural protein. J Virol **20:**307–313.
4. **Palese P, Ritchey MB, Schulman JL.** 1977. Mapping of the influenza virus genome. II. Identification of the P1, P2, and P3 genes. Virology **76:**114–121.
5. **Lamb RA, Lai CJ, Choppin PW.** 1981. Sequences of mRNAs derived from genome RNA segment 7 of influenza virus: colinear and interrupted mRNAs code for overlapping proteins. Proc Natl Acad Sci U S A **78:**4170–4174. http://dx.doi.org/10.1073/pnas.78.7.4170.
6. **Inglis SC, Barrett T, Brown CM, Almond JW.** 1979. The smallest genome RNA segment of influenza virus contains two genes that may overlap. Proc Natl Acad Sci U S A **76:**3790–3794. http://dx.doi.org/10.1073/pnas.76.8.3790.
7. **Lamb RA, Choppin PW.** 1979. Segment 8 of the influenza virus genome is unique in coding for two polypeptides. Proc Natl Acad Sci U S A **76:**4908–4912. http://dx.doi.org/10.1073/pnas.76.10.4908.
8. **Lamb RA, Choppin PW, Chanock RM, Lai CJ.** 1980. Mapping of the two overlapping genes for polypeptides NS1 and NS2 on RNA segment 8 of influenza virus genome. Proc Natl Acad Sci U S A **77:**1857–1861. http://dx.doi.org/10.1073/pnas.77.4.1857.
9. **Porter AG, Smith JC, Emtage JS.** 1980. Nucleotide sequence of influenza virus RNA segment 8 indicates that coding regions for NS1 and NS2 proteins overlap. Proc Natl Acad Sci U S A **77:**5074–5078. http://dx.doi.org/10.1073/pnas.77.9.5074.
10. **Lamb RA, Etkind PR, Choppin PW.** 1978. Evidence for a ninth influenza viral polypeptide. Virology **91:**60–78. http://dx.doi.org/10.1016/0042-6822(78)90355-0.
11. **Allen H, McCauley J, Waterfield M, Gething MJ.** 1980. Influenza virus RNA segment 7 has the coding capacity for two polypeptides. Virology **107:**548–551. http://dx.doi.org/10.1016/0042-6822(80)90324-4.
12. **Winter G, Fields S.** 1980. Cloning of influenza cDNA into M13: the sequence of the RNA segment encoding the A/PR/8/34 matrix protein. Nucleic Acids Res **8:**1965–1974. http://dx.doi.org/10.1093/nar/8.9.1965.
13. **Lamb RA, Choppin PW.** 1981. Identification of a second protein (M2) encoded by RNA segment 7 of influenza virus. Virology **112:**729–737. http://dx.doi.org/10.1016/0042-6822(81)90317-2.
14. **Lamb RA, Lai CJ.** 1981. Conservation of the influenza virus membrane protein (M1) amino acid sequence and an open reading frame of RNA segment 7 encoding a second protein (M2) in H1N1 and H3N2 strains. Virology **112:**746–751. http://dx.doi.org/10.1016/0042-6822(81)90319-6.
15. **Wise HM, Hutchinson EC, Jagger BW, Stuart AD, Kang ZH, Robb N, Schwartzman LM, Kash JC, Fodor E, Firth AE, Gog JR, Taubenberger JK, Digard P.** 2012. Identification of a novel splice variant form of the influenza A virus M2 ion channel with an antigenically distinct ectodomain. PLoS Pathog **8:**e1002998. http://dx.doi.org/10.1371/journal.ppat.1002998.
16. **Selman M, Dankar SK, Forbes NE, Jia JJ, Brown EG.** 2012. Adaptive mutation in influenza A virus non-structural gene is linked to host switching and induces a novel protein by alternative splicing. Emerg Microbes Infect **1:**e42. http://dx.doi.org/10.1038/emi.2012.38.
17. **Chen W, Calvo PA, Malide D, Gibbs J, Schubert U, Bacik I, Basta S, O'Neill R, Schickli J, Palese P, Henklein P, Bennink JR, Yewdell JW.** 2001. A novel influenza A virus mitochondrial protein that induces cell death. Nat Med **7:**1306–1312. http://dx.doi.org/10.1038/nm1201-1306.
18. **Wise HM, Foeglein A, Sun J, Dalton RM, Patel S, Howard W, Anderson EC, Barclay WS, Digard P.** 2009. A complicated message: identification of a novel PB1-related protein translated from influenza A virus segment 2 mRNA. J Virol **83:**8021–8031. http://dx.doi.org/10.1128/JVI.00826-09.
19. **Wise HM, Barbezange C, Jagger BW, Dalton RM, Gog JR, Curran MD, Taubenberger JK, Anderson EC, Digard P.** 2011. Overlapping signals for translational regulation and packaging of influenza A virus segment 2. Nucleic Acids Res **39:**7775–7790. http://dx.doi.org/10.1093/nar/gkr487.
20. **Akkina RK.** 1990. Antigenic reactivity and electrophoretic migrational heterogeneity of the three polymerase proteins of type A human and animal influenza viruses. Arch Virol **111:**187–197. http://dx.doi.org/10.1007/BF01311053.
21. **Muramoto Y, Noda T, Kawakami E, Akkina R, Kawaoka Y.** 2013. Identification of novel influenza A virus proteins translated from PA mRNA. J Virol **87:**2455–2462. http://dx.doi.org/10.1128/JVI.02656-12.
22. **Gibbs JS, Malide D, Hornung F, Bennink JR, Yewdell JW.** 2003. The influenza A virus PB1-F2 protein targets the inner mitochondrial membrane via a predicted basic amphipathic helix that disrupts mitochondrial function. J Virol **77:**7214–7224. http://dx.doi.org/10.1128/JVI.77.13.7214-7224.2003.
23. **Varga ZT, Ramos I, Hai R, Schmolke M, Garcia-Sastre A, Fernandez-Sesma A, Palese P.** 2011. The influenza virus protein PB1-F2 inhibits the induction of type I interferon at the level of the MAVS adaptor protein. PLoS Pathog **7:**e1002067. http://dx.doi.org/10.1371/journal.ppat.1002067.
24. **Yoshizumi T, Ichinohe T, Sasaki O, Otera H, Kawabata S, Mihara K, Koshiba T.** 2014. Influenza A virus protein PB1-F2 translocates into mitochondria via Tom40 channels and impairs innate immunity. Nat Commun **5:**4713. http://dx.doi.org/10.1038/ncomms5713.
25. **Jagger BW, Wise HM, Kash JC, Walters KA, Wills NM, Xiao YL, Dunfee RL, Schwartzman LM, Ozinsky A, Bell GL, Dalton RM, Lo A, Efstathiou S, Atkins JF, Firth AE, Taubenberger JK, Digard P.** 2012. An overlapping protein-coding region in influenza A virus segment 3 modulates the host response. Science **337:**199–204. http://dx.doi.org/10.1126/science.1222213.
26. **Cartegni L, Chew SL, Krainer AR.** 2002. Listening to silence and understanding nonsense: exonic mutations that affect splicing. Nat Rev Genet **3:**285–298. http://dx.doi.org/10.1038/nrg775.
27. **Dubois J, Terrier O, Rosa-Calatrava M.** 2014. Influenza viruses and mRNA splicing: doing more with less. mBio **5:**e00070-14. http://dx.doi.org/10.1128/mBio.00070-14.
28. **Neumann G, Watanabe T, Ito H, Watanabe S, Goto H, Gao P, Hughes**

M, Perez DR, Donis R, Hoffmann E, Hobom G, Kawaoka Y. 1999. Generation of influenza A viruses entirely from cloned cDNAs. Proc Natl Acad Sci U S A **96:**9345–9350. http://dx.doi.org/10.1073/pnas.96.16.9345.
29. **Watanabe T, Kawakami E, Shoemaker JE, Lopes TJ, Matsuoka Y, Tomita Y, Kozuka-Hata H, Gorai T, Kuwahara T, Takeda E, Nagata A, Takano R, Kiso M, Yamashita M, Sakai-Tagawa Y, Katsura H, Nonaka N, Fujii H, Fujii K, Sugita Y, Noda T, Goto H, Fukuyama S, Watanabe S, Neumann G, Oyama M, Kitano H, Kawaoka Y.** 2014. Influenza virus-host interactome screen as a platform for antiviral drug development. Cell Host Microbe **16:**795–805. http://dx.doi.org/10.1016/j.chom.2014.11.002.
30. **Hatta M, Asano Y, Masunaga K, Ito T, Okazaki K, Toyoda T, Kawaoka Y, Ishihama A, Kida H.** 2000. Mapping of functional domains on the influenza A virus RNA polymerase PB2 molecule using monoclonal antibodies. Arch Virol **145:**1947–1961. http://dx.doi.org/10.1007/s007050070068.
31. **Workman CT, Yin Y, Corcoran DL, Ideker T, Stormo GD, Benos PV.** 2005. enoLOGOS: a versatile web tool for energy normalized sequence logos. Nucleic Acids Res **33:**W389–W392. http://dx.doi.org/10.1093/nar/gki439.
32. **Yamayoshi S, Noda T, Ebihara H, Goto H, Morikawa Y, Lukashevich IS, Neumann G, Feldmann H, Kawaoka Y.** 2008. Ebola virus matrix protein VP40 uses the COPII transport system for its intracellular transport. Cell Host Microbe **3:**168–177. http://dx.doi.org/10.1016/j.chom.2008.02.001.
33. **Yoneyama M, Suhara W, Fukuhara Y, Fukuda M, Nishida E, Fujita T.** 1998. Direct triggering of the type I interferon system by virus infection: activation of a transcription factor complex containing IRF-3 and CBP/p300. EMBO J **17:**1087–1095. http://dx.doi.org/10.1093/emboj/17.4.1087.
34. **Ozawa M, Fujii K, Muramoto Y, Yamada S, Yamayoshi S, Takada A, Goto H, Horimoto T, Kawaoka Y.** 2007. Contributions of two nuclear localization signals of influenza A virus nucleoprotein to viral replication. J Virol **81:**30–41. http://dx.doi.org/10.1128/JVI.01434-06.
35. **Yamayoshi S, Yamada S, Fukuyama S, Murakami S, Zhao D, Uraki R, Watanabe T, Tomita Y, Macken C, Neumann G, Kawaoka Y.** 2014. Virulence-affecting amino acid changes in the PA protein of H7N9 influenza A viruses. J Virol **88:**3127–3134. http://dx.doi.org/10.1128/JVI.03155-13.
36. **Kärber G.** 1931. Beitrag zur kollektiven Behandlung pharmakologischer Reihenversuche. Naunyn Schmiedebergs Arch Exp Pathol Pharmakol **162:**480–483. http://dx.doi.org/10.1007/BF01863914.
37. **Spearman C.** 1908. The method of 'right and wrong cases' ('constant stimuli') without Gauss's formulae. Br J Psychol **2:**227–242.
38. **Lamb RA, Lai CJ.** 1982. Spliced and unspliced messenger RNAs synthesized from cloned influenza virus M DNA in an SV40 vector: expression of the influenza virus membrane protein (M1). Virology **123:**237–256. http://dx.doi.org/10.1016/0042-6822(82)90258-6.
39. **Lamb RA, Lai CJ.** 1984. Expression of unspliced NS1 mRNA, spliced NS2 mRNA, and a spliced chimera mRNA from cloned influenza virus NS DNA in an SV40 vector. Virology **135:**139–147. http://dx.doi.org/10.1016/0042-6822(84)90124-7.
40. **Mount SM.** 1982. A catalogue of splice junction sequences. Nucleic Acids Res **10:**459–472. http://dx.doi.org/10.1093/nar/10.2.459.
41. **Mount SM.** 1983. RNA processing. Sequences that signal where to splice. Nature **304:**309–310.
42. **Mukaigawa J, Nayak DP.** 1991. Two signals mediate nuclear localization of influenza virus (A/WSN/33) polymerase basic protein 2. J Virol **65:**245–253.
43. **Graef KM, Vreede FT, Lau YF, McCall AW, Carr SM, Subbarao K, Fodor E.** 2010. The PB2 subunit of the influenza virus RNA polymerase affects virulence by interacting with the mitochondrial antiviral signaling protein and inhibiting expression of beta interferon. J Virol **84:**8433–8445. http://dx.doi.org/10.1128/JVI.00879-10.
44. **Carr SM, Carnero E, Garcia-Sastre A, Brownlee GG, Fodor E.** 2006. Characterization of a mitochondrial-targeting signal in the PB2 protein of influenza viruses. Virology **344:**492–508. http://dx.doi.org/10.1016/j.virol.2005.08.041.
45. **Iwai A, Shiozaki T, Kawai T, Akira S, Kawaoka Y, Takada A, Kida H, Miyazaki T.** 2010. Influenza A virus polymerase inhibits type I interferon induction by binding to interferon beta promoter stimulator 1. J Biol Chem **285:**32064–32074. http://dx.doi.org/10.1074/jbc.M110.112458.
46. **Yoneyama M, Kikuchi M, Natsukawa T, Shinobu N, Imaizumi T, Miyagishi M, Taira K, Akira S, Fujita T.** 2004. The RNA helicase RIG-I has an essential function in double-stranded RNA-induced innate antiviral responses. Nat Immunol **5:**730–737. http://dx.doi.org/10.1038/ni1087.
47. **Pichlmair A, Schulz O, Tan CP, Naslund TI, Liljestrom P, Weber F, Reis e Sousa C.** 2006. RIG-I-mediated antiviral responses to single-stranded RNA bearing 5′-phosphates. Science **314:**997–1001. http://dx.doi.org/10.1126/science.1132998.
48. **Mibayashi M, Martinez-Sobrido L, Loo YM, Cardenas WB, Gale M, Jr, Garcia-Sastre A.** 2007. Inhibition of retinoic acid-inducible gene I-mediated induction of beta interferon by the NS1 protein of influenza A virus. J Virol **81:**514–524. http://dx.doi.org/10.1128/JVI.01265-06.
49. **Perales B, de la Luna S, Palacios I, Ortin J.** 1996. Mutational analysis identifies functional domains in the influenza A virus PB2 polymerase subunit. J Virol **70:**1678–1686.
50. **Poole E, Elton D, Medcalf L, Digard P.** 2004. Functional domains of the influenza A virus PB2 protein: identification of NP- and PB1-binding sites. Virology **321:**120–133. http://dx.doi.org/10.1016/j.virol.2003.12.022.
51. **Biswas SK, Nayak DP.** 1996. Influenza virus polymerase basic protein 1 interacts with influenza virus polymerase basic protein 2 at multiple sites. J Virol **70:**6716–6722.
52. **Hemerka JN, Wang D, Weng Y, Lu W, Kaushik RS, Jin J, Harmon AF, Li F.** 2009. Detection and characterization of influenza A virus PA-PB2 interaction through a bimolecular fluorescence complementation assay. J Virol **83:**3944–3955. http://dx.doi.org/10.1128/JVI.02300-08.
53. **Sugiyama K, Obayashi E, Kawaguchi A, Suzuki Y, Tame JR, Nagata K, Park SY.** 2009. Structural insight into the essential PB1-PB2 subunit contact of the influenza virus RNA polymerase. EMBO J **28:**1803–1811. http://dx.doi.org/10.1038/emboj.2009.138.
54. **York A, Fodor E.** 2013. Biogenesis, assembly, and export of viral messenger ribonucleoproteins in the influenza A virus infected cell. RNA Biol **10:**1274–1282. http://dx.doi.org/10.4161/rna.25356.
55. **Biswas SK, Boutz PL, Nayak DP.** 1998. Influenza virus nucleoprotein interacts with influenza virus polymerase proteins. J Virol **72:**5493–5501.
56. **Ohtsu Y, Honda Y, Sakata Y, Kato H, Toyoda T.** 2002. Fine mapping of the subunit binding sites of influenza virus RNA polymerase. Microbiol Immunol **46:**167–175. http://dx.doi.org/10.1111/j.1348-0421.2002.tb02682.x.
57. **Detjen BM, St Angelo C, Katze MG, Krug RM.** 1987. The three influenza virus polymerase (P) proteins not associated with viral nucleocapsids in the infected cell are in the form of a complex. J Virol **61:**16–22.
58. **Kato A, Mizumoto K, Ishihama A.** 1985. Purification and enzymatic properties of an RNA polymerase-RNA complex from influenza virus. Virus Res **3:**115–127. http://dx.doi.org/10.1016/0168-1702(85)90002-4.
59. **Fodor E, Smith M.** 2004. The PA subunit is required for efficient nuclear accumulation of the PB1 subunit of the influenza A virus RNA polymerase complex. J Virol **78:**9144–9153. http://dx.doi.org/10.1128/JVI.78.17.9144-9153.2004.
60. **Naito T, Momose F, Kawaguchi A, Nagata K.** 2007. Involvement of Hsp90 in assembly and nuclear import of influenza virus RNA polymerase subunits. J Virol **81:**1339–1349. http://dx.doi.org/10.1128/JVI.01917-06.
61. **Taubenberger JK, Reid AH, Lourens RM, Wang R, Jin G, Fanning TG.** 2005. Characterization of the 1918 influenza virus polymerase genes. Nature **437:**889–893. http://dx.doi.org/10.1038/nature04230.
62. **Vana G, Westover KM.** 2008. Origin of the 1918 Spanish influenza virus: a comparative genomic analysis. Mol Phylogenet Evol **47:**1100–1110. http://dx.doi.org/10.1016/j.ympev.2008.02.003.
63. **Novel Swine-Origin Influenza A (H1N1) Virus Investigation Team, Dawood FS, Jain S, Finelli L, Shaw MW, Lindstrom S, Garten RJ, Gubareva LV, Xu X, Bridges CB, Uyeki TM.** 2009. Emergence of a novel swine-origin influenza A (H1N1) virus in humans. N Engl J Med **360:**2605–2615. http://dx.doi.org/10.1056/NEJMoa0903810.